Lawrence Berkeley National Laboratory
LBL Publications

Title
Gas-phase formation of the resonantly stabilized 1-indenyl (C9H7•) radical in the interstellar medium.

Permalink
https://escholarship.org/uc/item/8622j89n

Journal
Science Advances, 9(36)

Authors
Yang, Zhenghai
Galimova, Galiya
He, Chao
et al.

Publication Date
2023-09-08

DOI
10.1126/sciadv.adi5060

Peer reviewed

eScholarship.org Powered by the California Digital Library
University of California

CHEMICAL PHYSICS

Gas-phase formation of the resonantly stabilized 1-indenyl ($C_9H_7^•$) radical in the interstellar medium

Zhenghai Yang[1]†, Galiya R. Galimova[2]†, Chao He[1]†, Shane J. Goettl[1], Dababrata Paul[1], Wenchao Lu[3], Musahid Ahmed[3]*, Alexander M. Mebel[2]*, Xiaohu Li[4,5]*, Ralf I. Kaiser[1]*

Copyright © 2023 The Authors, some rights reserved; exclusive licensee American Association for the Advancement of Science. No claim to original U.S. Government Works. Distributed under a Creative Commons Attribution NonCommercial License 4.0 (CC BY-NC).

The 1-indenyl ($C_9H_7^•$) radical, a prototype aromatic and resonantly stabilized free radical carrying a six- and a five-membered ring, has emerged as a fundamental molecular building block of nonplanar polycyclic aromatic hydrocarbons (PAHs) and carbonaceous nanostructures in deep space and combustion systems. However, the underlying formation mechanisms have remained elusive. Here, we reveal an unconventional low-temperature gas-phase formation of 1-indenyl via barrierless ring annulation involving reactions of atomic carbon [C(^{3}P)] with styrene ($C_6H_5C_2H_3$) and propargyl ($C_3H_3^•$) with phenyl ($C_6H_5^•$). Macroscopic environments like molecular clouds act as natural low-temperature laboratories, where rapid molecular mass growth to 1-indenyl and subsequently complex PAHs involving vinyl side-chained aromatics and aryl radicals can occur. These reactions may account for the formation of PAHs and their derivatives in the interstellar medium and carbonaceous chondrites and could close the gap of timescales of their production and destruction in our carbonaceous universe.

INTRODUCTION

For the past decade, resonantly stabilized free radicals (RSFRs), organic open-shell transients in which the unpaired electron is delocalized over the carbon skeleton, have emerged as fundamental molecular building blocks to polycyclic aromatic hydrocarbons (PAHs) and carbonaceous nanoparticles in combustion processes and in the interstellar medium (ISM) (*1*–*6*). Reaction pathways from RSFRs such as propargyl ($C_3H_3^•$), cyclopentadienyl ($C_5H_5^•$), benzyl ($C_7H_7^•$), and 1-indenyl ($C_9H_7^•$) (fig. S1A) to complex PAHs like pyrene ($C_{16}H_{10}$), fluoranthene ($C_{16}H_{10}$), and chrysene ($C_{18}H_{12}$) have been investigated (*5*, *6*). However, the presence of PAHs along with their derivatives such as ionized, hydrogenated, and side-chain substituted counterparts in the ISM and carbonaceous chondrites such as Allende, Orgueil, and Murchison still represents a critical paradox in our Universe (*7*–*9*). Timescales of PAH injection from carbon-rich circumstellar envelopes exceed a few 10^9 years, but the lifetimes of PAHs in deep space are limited by degradation through interstellar shocks, ultraviolet photons, and galactic cosmic rays to only a few 10^8 years (*10*–*12*). In essence, PAHs are destroyed faster than synthesized in carbon-rich asymptotic giant branch stars (*12*) along with planetary nebulae as their descendants (*13*). Hence, PAHs should not be observable via, e.g., unidentified infrared emissions (*14*), in the range from 3 to 14 μm, and diffuse interstellar bands′ discrete emission lines covering the visible (400 nm) to the near-infrared region (1.2 μm) (*15*) of the electromagnetic spectrum.

Rapid molecular mass growth processes involving RSFRs signify a solution to this puzzle through the synthesis of PAHs in cold molecular clouds at temperatures as low as 10 K (*2*, *8*, *16*). Supported by recent observations of the propargyl radical in the Taurus molecular cloud (TMC-1) (*17*, *18*), RSFRs can reach high fractional abundances of up to a few 10^{-8} with respect to molecular hydrogen. RSFRs hold lifetimes longer than nonresonantly stabilized hydrocarbon radicals due to the delocalization of the unpaired electron over (part of) the carbon backbone (*19*) and can undergo rapid radical-radical recombination reactions (*20*, *21*). However, whereas molecular beam experiments (*22*, *23*) and astrochemical modeling (*17*, *18*) provided compelling evidence on the formation of the simplest RSFR in TMC-1, propargyl ($C_3H_3^•$), via the bimolecular reaction of atomic carbon [C(^{3}P)] with ethylene (C_2H_4), reaction pathways to more complex RSFRs are largely unknown (*24*). This knowledge is of particular importance for the 1-indenyl ($C_9H_7^•$) radical (*25*). As a prototype of an aromatic and RSFR, the bicyclic, fused C5-C6 species represents the key building block of nonplanar PAHs such as corannulene ($C_{20}H_{10}$), nanobowls ($C_{40}H_{10}$), and fullerenes (C_{60} and C_{70}) (fig. S1B) with the five-membered ring in the carbon backbone curving the carbon skeleton out of plane (*26*, *27*). Therefore, an unraveling of the synthetic routes of the 1-indenyl ($C_9H_7^•$) radical is critical to constrain the population of PAHs delivered from reactions of RSFRs in our Universe.

Here, by exploiting molecular beams experiments (crossed molecular beams; chemical reactor) along with electronic structure calculations and astrochemical modeling, we provide persuasive evidence on the gas-phase formation of the 1-indenyl ($C_9H_7^•$; X^2A_2) radical through the elementary reaction of atomic carbon (C; ^{3}P) with styrene (C_8H_8; X^1A') (Reaction 1) and via the radical-radical reaction of propargyl ($C_3H_3^•$; X^2B_1) with phenyl ($C_6H_5^•$; X^2A_1) (Reaction 2) (fig. S2). These bimolecular reactions are barrierless and exoergic with all transition states residing lower than the energies of the separated reactants and could proceed rapidly even at molecular cloud conditions of 10 K. These reactions may provide facile routes to 1-indenyl ($C_9H_7^•$) via cyclization and aromatization reactions at astronomically observable fractional abundances of $(6.1 \pm 3.5) \times 10^{-11}$ with respect to molecular hydrogen in the TMC-1. As a prototype of an aromatic RSFR, 1-indenyl can undergo molecular mass growth processes

[1]Department of Chemistry, University of Hawaii at Manoa, 2545 McCarthy Mall, Honolulu, HI 96822, USA. [2]Department of Chemistry and Biochemistry, Florida International University, Miami, FL 33199, USA. [3]Chemical Sciences Division, Lawrence Berkeley National Laboratory, Berkeley, CA 94720, USA. [4]Xinjiang Astronomical Observatory, Chinese Academy of Sciences, Urumqi, Xinjiang 830011, P. R. China. [5]Key Laboratory of Radio Astronomy, Chinese Academy of Sciences, Urumqi, Xinjiang 830011, P. R. China.
*Corresponding author. Email: ralfk@hawaii.edu (R.I.K.); mebela@fiu.edu (A.M.M.); mahmed@lbl.gov (M.A.); xiaohu.li@xao.ac.cn (X.L.)
†These authors contributed equally to this work.

leading to more complex aromatic structures such as naphthalene ($C_{10}H_8$) (*3*), phenanthrene ($C_{14}H_{10}$) (*4*), pyrene ($C_{16}H_{10}$), and fluoranthene ($C_{16}H_{10}$) (*5*). Whereas in low-temperature interstellar environments, single-collision conditions dominate (*28*), elevated pressures such as in hydrocarbon-rich atmospheres of planets and their moons like Titan facilitate a three-body collisional stabilization of the reaction intermediate(s) with the buffer molecules like molecular nitrogen (N_2) (*29*, *30*). Thus, the route to indene (C_9H_8) formation is opened. These third-body stabilization processes also become increasingly important in high-pressure combustion settings with indene (C_9H_8) ubiquitously identified in hydrocarbon flames of, e.g., ethane (*31*), n-butane (*32*), and benzene (*33*). This investigation fills a critical gap in our knowledge of the underlying elementary mechanisms leading to (aromatic) RSFRs in extreme environments by exploiting the 1-indenyl ($C_9H_7^{\bullet}$) radical as a benchmark. These reactions eventually lead to nonplanar PAHs and carbonaceous nanostructures (carbonaceous grains) acting as molecular factories for biorelevant complex organics like amino acids and sugars in deep space (*16*), thus fundamentally enhancing our understanding of the chemical evolution of carbonaceous matter in the Universe (*27*)

$$\mathrm{C\ (12\ amu) + C_8H_8\ (104\ amu)} \rightarrow \mathrm{C_9H_7^{\bullet}\ (115\ amu) + H^{\bullet}\ (1\ amu)} \quad (1)$$

$$\mathrm{C_3H_3^{\bullet}\ (39\ amu) + C_6H_5^{\bullet}\ (77\ amu)} \rightarrow \mathrm{C_9H_7^{\bullet}\ (115\ amu) + H^{\bullet}\ (1\ amu)} \quad (2)$$

RESULTS

Carbon-styrene system: Laboratory frame

The crossed molecular beam studies of ground state atomic carbon (C; 12 amu) with styrene ($C_6H_5C_2H_3$; 104 amu) (Fig. 1, A and B, and Reaction 1) revealed reactive scattering signal at mass-to-charge (m/z) ratios of 116 ($C_9H_8^+/^{13}CC_8H_7^+$), 115 ($C_9H_7^+/^{13}CC_8H_6^+$), and 114 ($C_9H_6^+/^{13}CC_8H_5^+$). Ion counts at m/z = 116 and 114 were collected at a level of 9 ± 2% and 78 ± 4% with respect to m/z = 115. Because the TOFs recorded at these m/z values are indistinguishable after scaling, we conclude the existence of a single H-loss reaction channel (Reaction 1). Ion counts at m/z = 116 originate from naturally abundant $^{13}CC_8H_6^+$, while m/z = 114 can be accounted for through dissociative electron impact ionization of the C_9H_7 neutral product in the electron impact ionizer to $C_9H_6^+$. The laboratory angular distribution (LAD) was, therefore, collected at m/z 115 from 28° to 66° in 2.5° intervals. This distribution spans about 40° within the scattering plane as defined by both beams and displays a forward-backward symmetry with a maximum at the center-of-mass (CM) angle of 52.8 ± 0.6°. This finding suggests indirect reaction dynamics via long-lived C_9H_8 intermediate(s) (Fig. 1, A and B). Because the hydrogen atom can be eliminated from the phenyl ($C_6H_5^{\bullet}$) group and/or from the vinyl moiety ($C_2H_3^{\bullet}$), crossed beam experiments were also conducted with D3- and D5-styrene, i.e., $C_6H_5C_2D_3$ and $C_6D_5C_2H_3$, respectively. These studies reveal that the atomic hydrogen loss can originate from both the vinyl moiety and the phenyl group (Materials and Methods).

CM frame

The interpretation of the laboratory data delivers conclusive evidence of the atomic hydrogen emission from both the vinyl moiety and the aromatic ring of styrene. It is our goal now to elucidate the underlying reaction mechanism(s) and to assign the C_9H_7 product isomer(s) formed in the bimolecular gas-phase reaction. This is accomplished by transforming the laboratory data into the CM frame (*34*), resulting in the CM translational energy distribution [$P(E_T)$] and the angular distribution [$T(\theta)$] (Fig. 1, C and D). Best fits of the laboratory data are achieved by exploiting a single-channel fit forming products with a mass combination of 115 amu (C_9H_7) and 1 amu (H). Crucial information on the reaction channel(s) and dynamics is derived through a detailed inspection of these CM functions. First, energy conservation dictates that the high energy cutoff of the $P(E_T)$ of 389 ± 24 kJ mol^{-1} presents the sum of the collision energy (35.4 ± 1.4 kJ mol^{-1}; table S1) plus the reaction exoergicity for those molecules born without internal excitation. Therefore, a reaction energy of 353 ± 25 kJ mol^{-1} is revealed. This experimentally derived exoergicity agrees well with the reaction exoergicity of 360 ± 5 kJ mol^{-1} to form the 1-indenyl radical ($C_9H_7^{\bullet}$) plus atomic hydrogen. Second, the $P(E_T)$ displays a pronounced distribution maximum of 20 ± 2 kJ mol^{-1}, revealing a tight exit transition state. Third, the $T(\theta)$ has an intensity over the complete angular range and reveals a forward-backward symmetry with a maximum at 90° (sideway scattering); these findings support indirect reaction dynamics involving C_9H_8 complex(es) with a lifetime longer than the rotational period, which undergoes unimolecular decomposition through atomic hydrogen loss nearly parallel to the total angular momentum vector (*34*).

Propargyl-phenyl system: Mass spectra

The reaction of propargyl ($C_3H_3^{\bullet}$) with the phenyl radical ($C_6H_5^{\bullet}$) was conducted in a chemical microreactor (*3*). The microreactor consists of a heated silicon carbide (SiC) tube and is incorporated within the source chamber of a molecular beam apparatus equipped with a Wiley-McLaren reflectron time-of-flight mass spectrometer (Re-TOF-MS). Thermally labile propargyl bromide (C_3H_3Br) and nitrosobenzene (C_6H_5NO) precursor molecules were seeded in helium carrier gas and pyrolyzed in situ through cleavage of the weak carbon-bromine and carbon-nitrogen bonds, respectively, producing selectively helium-seeded propargyl ($C_3H_3^{\bullet}$) (*20*) and phenyl radicals ($C_6H_5^{\bullet}$) (*35*) at a reactor temperature of 1373 ± 10 K (Materials and Methods). The reaction products were expanded supersonically and probed isomer-selectively via tunable vacuum ultraviolet (VUV) light from a synchrotron (*3*). Control experiments of only helium-seeded nitrosobenzene and only propargyl bromide under identical experimental conditions were conducted (*35*) too ("blank experiments") (Fig. 2A). Likewise, a representative mass spectrum recorded at a photon energy of 9.50 eV for the reaction of the phenyl ($C_6H_5^{\bullet}$) with propargyl ($C_3H_3^{\bullet}$) radical is displayed in Fig. 2B. A careful analysis of these mass spectra provides compelling evidence that the signal at m/z = 115 ($C_9H_7^+$) and 116 ($C_9H_8^+/^{13}CC_8H_7^+$) originates from the phenyl–propargyl radical–radical reaction but is absent in the control experiments. Accounting for the molecular weight of the reactants ($C_6H_5^{\bullet}$, 77 amu; $C_3H_3^{\bullet}$, 39 amu) and the products (C_9H_7, 115 amu; C_9H_8, 116 amu), molecules with the formula C_9H_7 are the reaction products of the reaction of propargyl ($C_3H_3^{\bullet}$) with phenyl ($C_6H_5^{\bullet}$) (Reaction 2) (fig. S2); the formation of C_9H_8 molecules

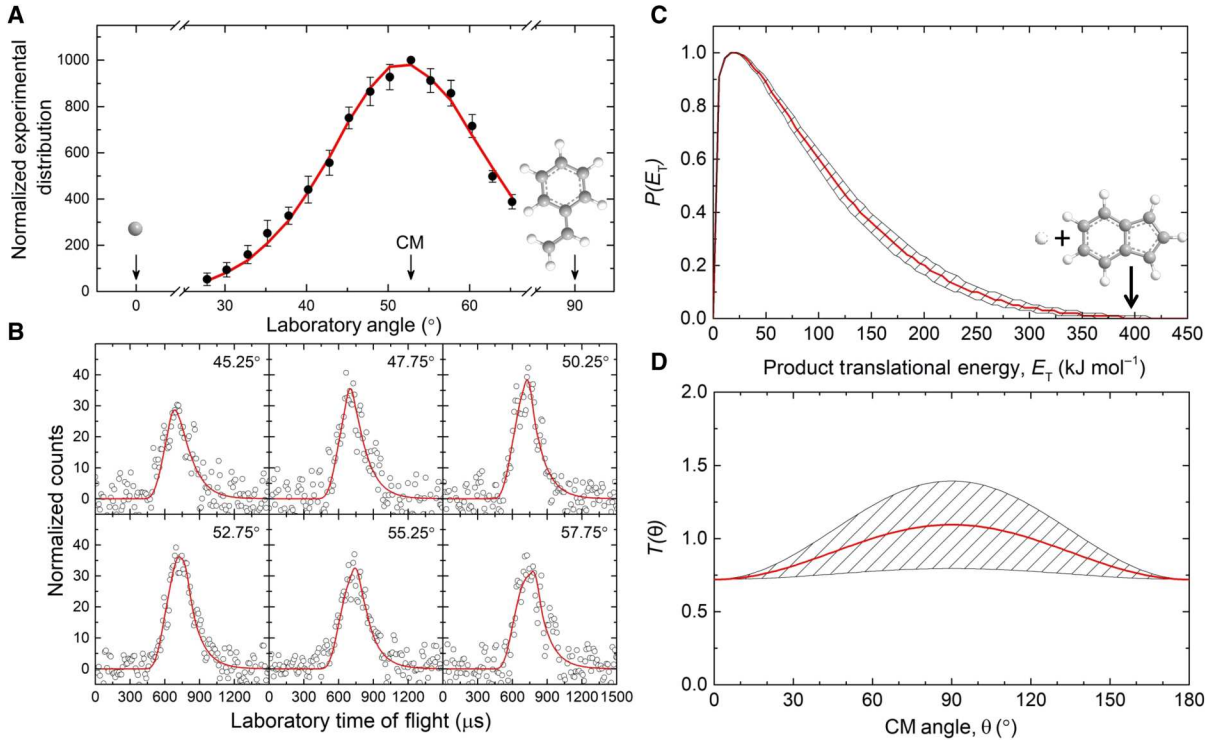

Fig. 1. Results for the reaction of atomic carbon (C) with styrene (C_8H_8). LAD (**A**), TOF spectra (**B**), CM translational energy (**C**), and angular flux distributions (**D**). Data are recorded at m/z = 115. The black circles with their error bars indicate the normalized experimental distribution, the open circles delineate the experimental data, the red lines represent the best fits obtained, and the shaded areas depict the error limits of the best fit.

can be linked to adducts and/or their isomerization products of the recombination of phenyl with propargyl radicals, which are then stabilized by a third-body reaction with helium (*20*).

Photoionization efficiency spectra

To unravel the nature of the isomer(s) formed, we turn to photoionization efficiency (PIE) curves, which report the intensity of a well-defined ion of a specific m/z ratio as a function of photon energy that is 7.50 to 10.0 eV in this case. The PIE curves for m/z = 116 ($C_9H_8^+/^{13}CC_8H_7^+$) (Fig. 2C) and 115 ($C_9H_7^+$) (Fig. 2D) can be reproduced via fitting with a linear combination of known reference curve(s) (*36*) of distinct isomer(s). First, the PIE curve at m/z = 116 can be replicated by the sum of four channels: 3-phenyl-1-propyne [$(C_6H_5)CH_2CCH$], phenylallene [$(C_6H_5)HCCCH_2$], indene (C_9H_8), and ^{13}C-indenyl ($^{13}CC_8H_7^+$) (Fig. 2C). Second, the experimentally derived PIE curve at m/z = 115 (Fig. 2D, black) can be reproduced by a single contributor, the 1-indenyl radical ($C_9H_7^•$, blue) (*37*, *38*). ^{13}C-indenyl ion counts contribute to a level of 9.9% with respect to that of 1-indenyl as shown in Fig. 2D. The onset of the ion counts at 8.10 ± 0.05 eV correlates well with the National Institute of Standards and Technology–evaluated adiabatic ionization energy (IE) of indene at 8.14 ± 0.01 eV (*39*); the adiabatic IE of 3-phenyl-1-propyne [$(C_6H_5)H_2CCCH$] and phenylallene [$(C_6H_5)HCCCH_2$] were determined to 8.75 ± 0.05 eV and 8.30 ± 0.05 eV, respectively (*40*). Therefore, we may conclude that, within our error limits, 3-phenyl-1-propyne, phenylallene, indene, and ^{13}C-indenyl contribute to signal at m/z = 116 with the branching ratios of the ion counts of 34 ± 2%, 24 ± 3%, 36 ± 2%, and 6 ± 3%, respectively. It is possible that 3-phenyl-1-propyne and phenylallene can undergo unimolecular decomposition via H loss to form the corresponding C_9H_7 radicals (m/z = 115), namely, 1-phenylpropargyl (1PPR; C_6H_5CHCCH) and 3-phenylpropargyl (3PPR; $C_6H_5CCCH_2$) radicals. From our fitting results, the match of the reference indenyl PIE with our experimental PIE curve of m/z = 115 demonstrates that indenyl should be the dominant product for m/z = 115 at our high-temperature experimental condition of 1373 ± 10 K. These results are supported by the recent kinetic calculations for the branching ratios for the C_6H_5 plus C_3H_3 reaction at different pressure and temperatures, which reveal that 1PPR and 3PPR are relatively minor products compared to 1-indenyl (*41*). Until now, there is very limited experimental PIE data for 1PPR and 3PPR (*37*). A comparison of the available experimental PIE of each reference radical with our experimental PIE curve of 115 is shown in fig. S3. Because the experimental PIE of 1PPR and 3PPR is recorded in a very short range of photon energy (7.5 to 7.8 eV for 3PPR and 7.5 to 9.0 eV for 1PPR), it is not possible to precisely calculate the branching ratios for the indenyl, 1PPR, and 3PPR.

Electronic structure calculations and reaction mechanisms: Carbon-styrene system

The electronic structure calculations of relative energies of local minima, transition states, and products were conducted at an accuracy of ±5 kJ mol^{-1} (Fig. 3) (*42*, *43*) and reveal that the reaction of atomic carbon with styrene can be initiated on the triplet surface through a barrierless addition of the carbon atom to the π electron density of the carbon-carbon double bond of the vinyl moiety (C_2H_3). This addition leads to a phenyl-substituted triplet

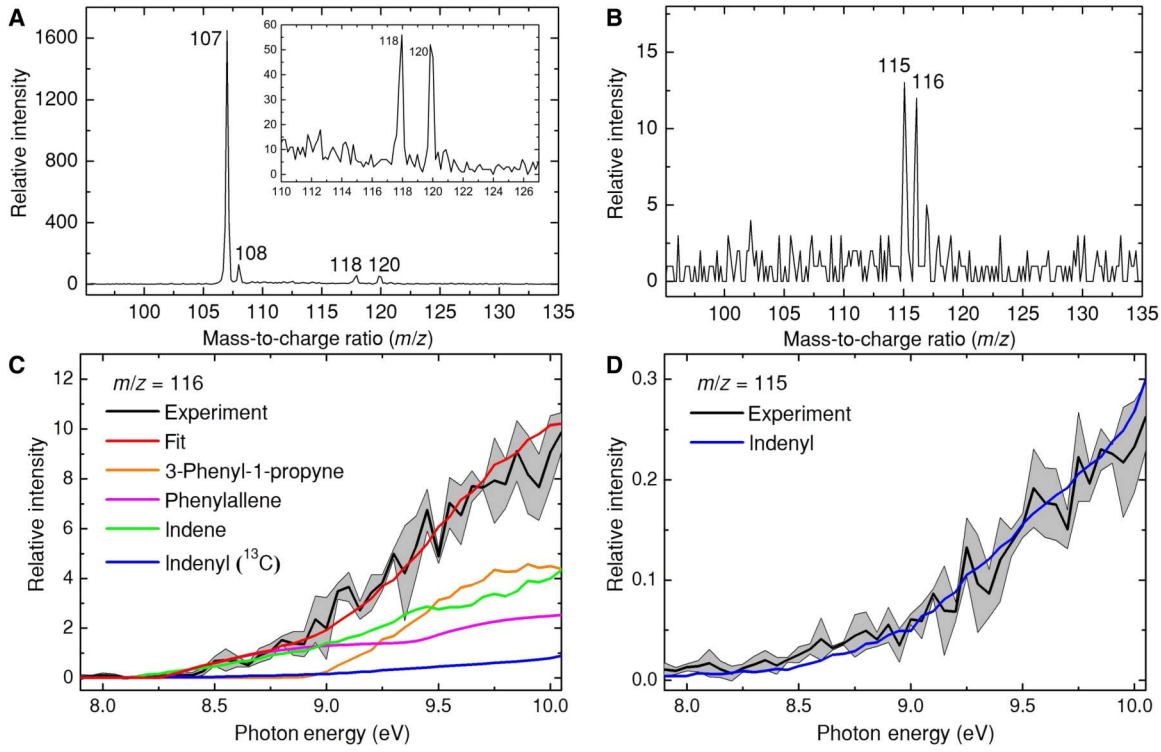

Fig. 2. Results for the phenyl ($C_6H_5^{\bullet}$) with propargyl ($C_3H_3^{\bullet}$) reaction. Photoionization mass spectra recorded at a photon energy of 9.50 eV with mass values of 107 ($C_6H_5NO^+$), 108 ($^{13}CC_5H_5NO^+$), 118 ($C_3H_3{}^{79}Br^+$), and 120 ($C_3H_3{}^{81}Br^+$); the inset highlights ion signal from m/z = 110 to 127 (**A**). Photoionization mass spectra recorded at 9.50 eV and 1373 ± 10 K (**B**). Photoionization efficiency (PIE) curves recorded at 116 (**C**) and 115 (**D**) for products of interest formed at a reactor temperature of 1373 ± 10 K. The black/blue/green/orange/magenta lines in (C) and (D) represent experimental and reference PIE curves, and the red line resembles the overall fit. The error bars consist of two parts: ±10% based on the accuracy of the photodiode and a 1 σ error of the PIE curve averaged over the individual scans.

cyclopropylidene intermediate **i1** stabilized by 225 kJ mol^{-1} with respect to the separated reactants. In analogy to the reaction with the stem compound ethylene (C_2H_4) (*44*, *45*), the computations also predict that insertion of atomic carbon into any carbon-hydrogen bond of the vinyl or phenyl functional groups is closed. **i1** ring opens via a barrier of only 36 kJ mol^{-1} to the thermodynamically preferred triplet phenylallene (**i2**). Four reaction pathways are opened from **i2**: a hydrogen migration from the ortho position of the phenyl ring to the C2 of the side chain forming **i3**, a 1,2-H migration in the side chain to phenyl-substituted triplet vinylmethylene (**i5**), and two unimolecular decompositions via H loss from the CH and CH_2 moieties forming 3-phenylpropargyl (**p3**) and 1-phenylpropargyl (**p2**) radicals via tight exit transition states. Commencing with **i3**, cis-trans isomerization of the side chain leads to **i4**; this is followed by hydrogen migration from the C1 carbon atom of the side chain to the ortho carbon atom of the aromatic ring yielding **i5**, which can further isomerize via cis-trans isomerization to **i6**. **i6** can unimolecularly decompose via atomic hydrogen elimination to 1-phenylpropargyl (**p2**) or undergo cyclization to the bicyclic 3aH-indene intermediate (**i7**). This bicyclic intermediate can lose a hydrogen atom to form 1-indenyl (**p1**) or isomerize via hydrogen atom migration to triplet indene (**i8**) before hydrogen atom elimination from the CH_2 moiety to 1-indenyl (**p1**). Both pathways involve tight exit transition states of 35 and 60 kJ mol^{-1} with respect to the separated products with the **i7** → **i8** → **p1** + H pathway unfavorable compared to **i7** → **p1** + H due to the high barrier of 163 kJ mol^{-1} for the hydrogen atom migration.

How do these results compare to our experimental findings? First, the experimentally determined reaction exoergicity for the hydrogen atom loss to C_9H_7 isomers of −353 ± 25 kJ mol^{-1} agrees well with the computed data of −360 ± 5 kJ mol^{-1} to yield 1-indenyl (**p1**) plus atomic hydrogen. Therefore, we can conclude that at least the indenyl radical ($C_9H_7^{\bullet}$, **p1**) is formed in the bimolecular reaction of atomic carbon with styrene. The presence of the theromodynamically less stable isomers 1-phenylpropargyl (**p2**; −217 ± 5 kJ mol^{-1}) and 3-phenylpropargyl (**p3**; −208 ± 5 kJ mol^{-1}) can be masked in the low energy section of the CM translational energy distribution. This conclusion also gains support from statistical calculations with Rice-Ramsperger-Kassel-Marcus (RRKM) theory (Materials and Methods) to predict branching ratios within the limits of complete energy randomization (*42*). This treatment predicts that 1-indenyl (**p1**) contributes to 54.9% of all products, whereas 1-phenylpropargyl (**p2**) and 3-phenylpropargyl (**p3**) account for 41.6 and 3.5%, respectively. It shall be highlighted that alternative indenyl isomers, i.e., 2-indenyl (144 kJ mol^{-1}), 3-indenyl (145 kJ mol^{-1}), 4-indenyl (133 kJ mol^{-1}), 5-indenyl (132 kJ mol^{-1}), 6-indenyl (133 kJ mol^{-1}), and 7-indenyl (132 kJ mol^{-1}), are thermodynamically less stable than 1-indenyl with relative energies indicated in the parentheses (*46*). Therefore, the formation of 2- to 7-indenyl cannot account for the experimentally derived reaction energy.

Second, the $P(E_T)$ reveals a tight exit transition state in the decomposition of C_9H_8 reaction intermediate(s). The presence of a tight exit transition state is verified computationally for the pathways **i7** → **i8** → **p1** + H and **i7** → **p1** + H. The reverse reaction,

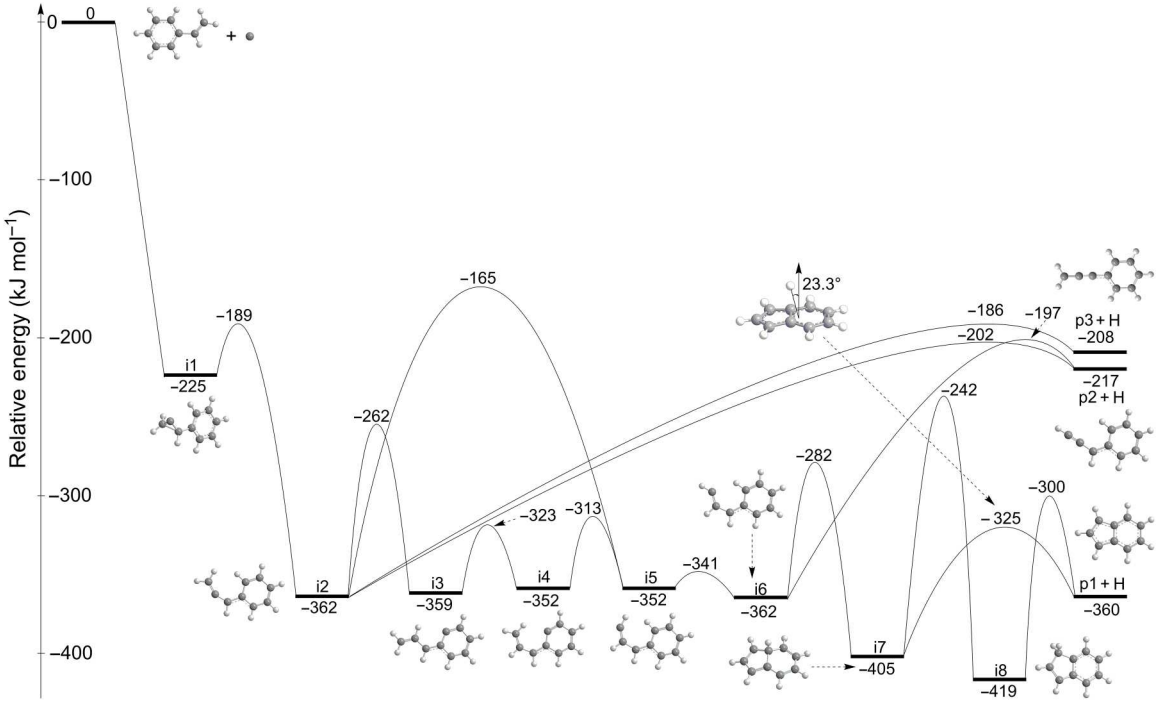

Fig. 3. Potential energy surfaces of the C + C_8H_8 reaction. Potential energy surface for the reaction of ground-state atomic carbon (C; ^{3}P) with styrene (C_8H_8; X^1A'). All energies are given in kilojoules per mole with respect to the energy of the separated reactants.

i.e., the recombination of atomic hydrogen with 1-indenyl (**p1**), formally represents a radical-radical reaction and hence should proceed via atom-radical recombination without an entrance barrier if this reaction proceeds on the singlet surface (*47*, *48*). However, the experimental evidence of a tight exit transition state supports our computations that the reaction proceeds on the triplet surface without intersystem crossing to the singlet manifold.

Third, the sideway scattering is evident from the computed structure of the transition state associated with the fragmentation of **i7** to **p1** + H (Fig. 3) with the atomic hydrogen leaving nearly perpendicularly to the rotational plane of the decomposing **i7** intermediate. Note that the RRKM calculations also predict that 99% of 1-indenyl (**p1**) originates from **i7** → **p1** + H and less than 1% from **i7** → **i8** → **p1** + H.

Last, we would like to address the experimental findings of the isotopic substitution studies in light of the computed surface (Fig. 3 and figs. S4 and S5). Branching ratios of the four pathways—(i) **i2** → **p3** + H (3.5%), (ii) **i2** → **p2** + H (29.5%), (iii) **i6** → **p2** + H (12.1%), and (iv) **i7** → **p1** + H (54.7%)—along with the dominance of 1-indenyl (**p1**; 54.9%) and 1-phenylpropargyl (**p2**; 41.6%) are predicted via the RRKM calculations (table S2). Considering these pathways, the predicted ratio of the hydrogen atom loss from the phenyl group versus the vinyl moiety is 1.22 ± 0.03:1. The isotopic experiments also determined the extent of the hydrogen loss in the $C/C_6H_5C_2D_3$ (from the phenyl group; fig. S4) and $C/C_6D_5C_2H_3$ systems (from the vinyl group; fig. S5) detected at m/z = 120 and 118, respectively, to be 1.18 ± 0.02:1 (Supplementary Materials). This result is in excellent agreement with the RRKM calculations, suggesting that, to eventually eliminate atomic hydrogen, the carbon atom preferentially attacks initially the vinyl moiety, but not the aromatic ring.

Considering the larger cone of acceptance of the aromatic ring compared to the vinyl group, these findings seem counterintuitive. Furthermore, atomic carbon was found to react with the benzene molecule (C_6H_6) (*49*) forming the cyclic 1,2-didehydrocycloheptatrienyl radical ($C_7H_5^{\bullet}$) plus atomic hydrogen. This reaction has neither an entrance nor an exit barrier and is only weakly exoergic by 8 kJ mol^{-1}. In the present situation, the reaction of atomic carbon with the aromatic ring of styrene has two competing exit channels: a vinyl radical ($C_2H_3^{\bullet}$) loss forming the cyclic 1,2-didehydrocycloheptatrienyl radical ($C_7H_5^{\bullet}$) (fig. S6, **p4**) as the heavy cofragment (Reaction 3) and an atomic hydrogen loss leading to three distinct vinyl-1,2-didehydrocycloheptatrienyl radicals (Reaction 4) (fig. S6, **p5** to **p7**). The reactions are only slightly exoergic, by 19 kJ mol^{-1} ($C_7H_5^{\bullet}$ plus $C_2H_3^{\bullet}$) and by 40, 6, and 15 kJ mol^{-1} for the vinyl-1,2-didehydrocycloheptatrienyl ($C_7H_4C_2H_3^{\bullet}$) plus atomic hydrogen channel depending on the position of the de facto carbon atom insertion via addition − ring opening into the six-membered ring of styrene with respect to the vinyl group. Therefore, we may conclude that, although Reactions 3 and 4 are feasible, they are much less favorable thermodynamically than the formation of 1-indenyl (**p1**) and 1-/3-phenylpropargyl (**p2**/**p3**). Reaction 4 cannot be responsible for the experimentally observed translational energy distribution.

$$C(^3P) + C_6H_5C_2H_3 \rightarrow C_7H_5^{\bullet} + C_2H_3^{\bullet} \quad (3)$$

$$C(^3P) + C_6H_5C_2H_3 \rightarrow C_7H_4C_2H_3^{\bullet} + H^{\bullet} \quad (4)$$

Propargyl-phenyl system

Having elucidated the formation of 1-indenyl ($C_9H_7^•$) in the reaction of atomic carbon with styrene, we now turn our attention to the propargyl-phenyl system (Fig. 4). According to the previous calculations (*48*), the reaction is initiated by the barrierless addition of the propargyl radical's CH_2 or CH terminal moieties to the radical site of phenyl producing intermediates **i9** (3-phenyl-1-propyne) and **i10** (phenylallene), respectively. These isomers reside in deep potential energy wells and are stabilized by 381 and 400 kJ mol^{-1} with respect to the separated reactants. **i9** isomerizes via a hydrogen shift and ring closure forming the bicyclic intermediate **i11**. Two pathways are open from **i10**: (i) isomerization to **i11** via hydrogen atom migration from the terminal carbon at the CH_2 moiety and closure to a five-membered ring and (ii) isomerization to **i12** through atomic hydrogen shift from the phenyl ring to the side chain. Once formed, **i11** can further isomerize to indene (**i13**) via hydrogen migration or fragments to the 1-indenyl radical (**p8**) in an overall exoergic reaction. Alternatively, **i12** can undergo ring closure to indene (C_9H_8) with the latter ejecting an atomic hydrogen barrierlessly forming the 1-indenyl radical ($C_9H_7^•$). A close inspection of the PES reveals five reaction sequences to 1-indenyl ($C_9H_7^•$) with barriers located below the energy of the separated reactants. These pathways are, in principle, accessible even at ultralow temperatures of 10 K in the cold molecular cloud: **i9 → i11 → i13 → p8 + H**, **i10 → i11 → i13 → p8 + H**, **i9 → i11 → p8 + H**, **i10 → i11 → p8 + H**, and **i10 → i12 → i13 → p8 + H**. It should be stressed that these calculations support the experimental identification of the 1-indenyl radical ($C_9H_7^•$) and of three adducts—3-phenyl-1-propyne (**i9**), phenylallene (**i10**), and indene (**i13**)—with three-body collisions with the buffer gas (helium) required to stabilize these initial collision complexes. Recently, Couch *et al.* (*50*) and Selby *et al.* (*41*) studied the propargyl − phenyl reaction. Couch *et al.* (*50*) conducted the experiment in a continuous flow over the temperature range of 800 to 1600 K and pressures of 25 torr. The authors detected ions attributable to $C_9H_7^+$ and $C_9H_8^+$. However, the electron impact ionization could neither reveal the source of $C_9H_7^+$, i.e., nascent reaction product or dissociative electron impact ionization of C_9H_8, nor elucidate the nature of the structural isomers of C_9H_8. Selby *et al.* (*41*) studied this reaction over 300 to 1000 K and 4 to 10 torr using time-resolved multiplexed photoionization mass spectrometry. The isomer-resolved branching ratios for the C_9H_8 products are reported from 300 to 1000 K. On the basis of their photoionization spectra, at 300 K and 4 torr, only the direct C_9H_8 adducts 3-phenyl-1-propargyl and phenylallene are observed with the branching ratios of 77 ± 5% and 23 ± 3%, respectively. As the temperature and pressure are increased to 1000 K and 10 torr, respectively, two additional C_9H_8 isomers, 1-phenyl-1-propyne and indene, along with the C_9H_7 + H channel are observed. The corresponding branching fractions of C_9H_8 isomers are 61 ± 6%, 18 ± 3%, 6 ± 1%, and 15 ± 5% for 3-phenyl-1-propargyl, phenylallene, 1-phenyl-1-propyne, and indene, respectively. It should be noted that the C_9H_7 isomer distributions are not determined experimentally although it supplies 16 ± 5% of total C_9H_8 signal at 1000 K. Here, our experiment is conducted at much higher temperature and pressure of 1373 ± 10 K and 200 ± 10 torr exploiting a chemical microreactor and tunable synchrotron VUV light coupled with a Re-TOF-MS. Compared with the results from (*41*) under lower-temperature conditions, additional insights into the high-temperature chemistry of C_3H_3 + C_6H_5 reaction are derived. First, only three C_9H_8 isomers are observed at 116, namely, 3-phenyl-1-propyne (34 ± 2%), phenylallene (24 ± 3%), and indene (36 ± 2%). Second, 1-indenyl (C_9H_7) is determined to be the dominant product at 115 with 1PPR and 3PPR possibly being the minor products.

Astrochemical modeling

The identification of the 1-indenyl radical ($C_9H_7^•$) via the barrierless elementary reactions (Reactions 1 and 2) lends to an opportunity of incorporating these findings into astrochemical models of cold molecular clouds. It is vital to underline that both reactions have no entrance barriers, all barriers of the isomerization processes are below the energy of the separate reactants, and the overall reactions are exoergic. These findings denote key prerequisites for reactions to proceed in low-temperature environments such as in molecular clouds (10 K). To investigate the implications of our findings to the chemistry of 1-indenyl in cold molecular clouds, we untangled the viability of the formation of 1-indenyl through the neutral-neutral reactions (Reactions 1 and 2) using the University of Manchester Institute for Science and Technology Database (RATE2012) (*51*) operated with the two-step single-point time-dependent astrochemical model described in (*52*) and (*53*). The physical parameters of the models were updated according to Markwick

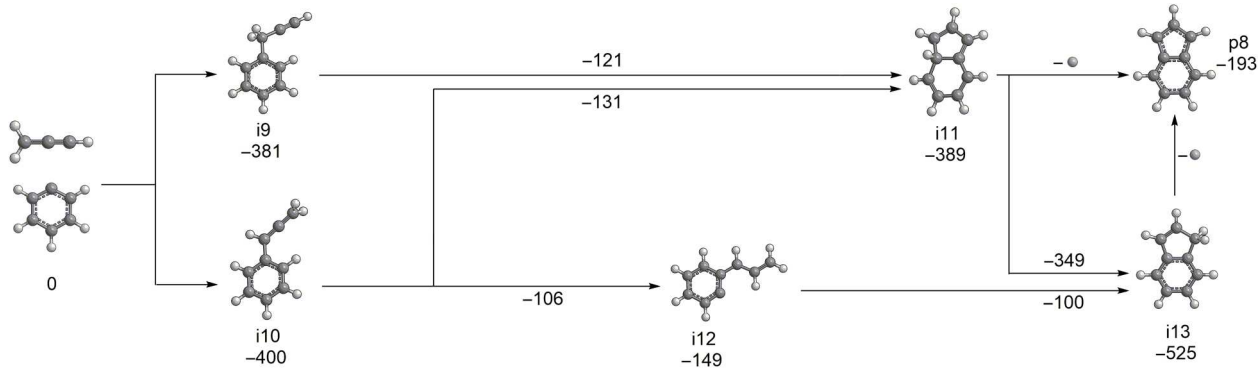

Fig. 4. Potential energy surfaces of the C_6H_5 + C_3H_3 reaction. Dominant reaction pathways for the phenyl ($C_6H_5^•$) with propargyl ($C_3H_3^•$) reaction extracted from (*48*). The values on top/bottom of the arrows indicate the energies of the transition states. All energies are given in kilojoules per mole with respect to the energy of the separated reactants.

et al. (*54*) and McElroy *et al.* (*51*); reaction rate coefficients and (pre-exponential) factor α (table S3) are parameterized according to McElroy *et al.* (*51*). The physical parameters of the cold molecular cloud are triggered by a temperature of 10 K, a cosmic ray ionization rate of 1.3×10^{-17} s^{-1}, a visual extinction of 10 Mag, and a number density of molecular hydrogen of 10^4 cm^{-3}. The chemical network was also enhanced with recently explored barrierless and rapid reactions related to the formation of propargyl (C_3H_3) (*22*), benzene (C_6H_6) (*52*), and indene (C_9H_8) (*27*). The key bimolecular reactions and photodissociation processes newly incorporated into the astrochemical model leading to the formation of 1-indenyl are shown in Fig. 5, and the details are depicted in table S3. In the simulations, the fiducial gas-phase model was first operated until the chemistry evolved to the steady state; then, the obtained molecular abundances at this point are used as the initial conditions for the second-step model where the ice mantle species are injected into the gas phase until the model reaches the steady state again. Last, the predictive capabilities of the model are verified by comparing the relevant species observed with modeled fractional abundances.

These modeling studies reveal captivating findings (Fig. 6 and fig. S7). First, the exceptional performance of the astrochemical model for TMC-1 can be well benchmarked for the propargyl (C_3H_3), cyanobenzene (C_6H_5CN), and indene (C_9H_8) recently detected at fractional abundances of 0.8×10^{-8} to 1.2×10^{-8} (*17*, *18*), 2.4×10^{-11} to 1.2×10^{-10} (*55*, *56*), and 7.6×10^{-10} to 1.0×10^{-9} (*57*, *58*) toward TMC-1. Prepared principally via the barrierless reactions of atomic carbon with ethylene (*22*) and of benzene with cyano radicals (*59*), the predicted peak fractional abundances of propargyl and cyanobenzene at 1.3×10^5 and 7.9×10^4 years of 2.9×10^{-9} to 1.1×10^{-8} and 4.1×10^{-11} to 4.7×10^{-11} with respect to molecular hydrogen replicate the astronomical observations exceptionally well (Fig. 6). A match between the modeled (1.0×10^{-10} to 9.0×10^{-10}) and observed fractional abundances (7.6×10^{-10} to 1.0×10^{-9}) has also been achieved for indene (C_9H_8) with dominating formation routes involving the reactions of methylidyne (CH) with styrene (C_8H_8) (*27*) and *o*-benzyne (C_6H_4) with allyl (C_3H_5) (*60*). Second, barrierless molecular mass growth processes via ring annulation were predicted to form 1-indenyl ($C_9H_7^{\bullet}$) peaking at fractional abundances of 2.4×10^{-11} to 9.7×10^{-11} at 2.5×10^5 years; Reactions 1 and 2 contribute nearly equally with 55 and 45%, respectively. These fractional abundances suggest that the 1-indenyl radical ($C_9H_7^{\bullet}$) might be detectable by radio telescopes such as the Green Bank Observatory (*61*) and Yebes Radio Telescope (*17*).

DISCUSSION

Our combined experimental, computational, and astrochemical modeling study provided compelling evidence on the very first gas-phase preparation of the aromatic and resonantly stabilized 1-indenyl ($C_9H_7^{\bullet}$) radical via elementary reactions of ground state atomic carbon (C) with styrene ($C_6H_5C_2H_3$) and of the propargyl radical ($C_3H_3^{\bullet}$) with the phenyl radical ($C_6H_5^{\bullet}$). These pathways provide unique access to 1-indenyl via barrierless entrance and

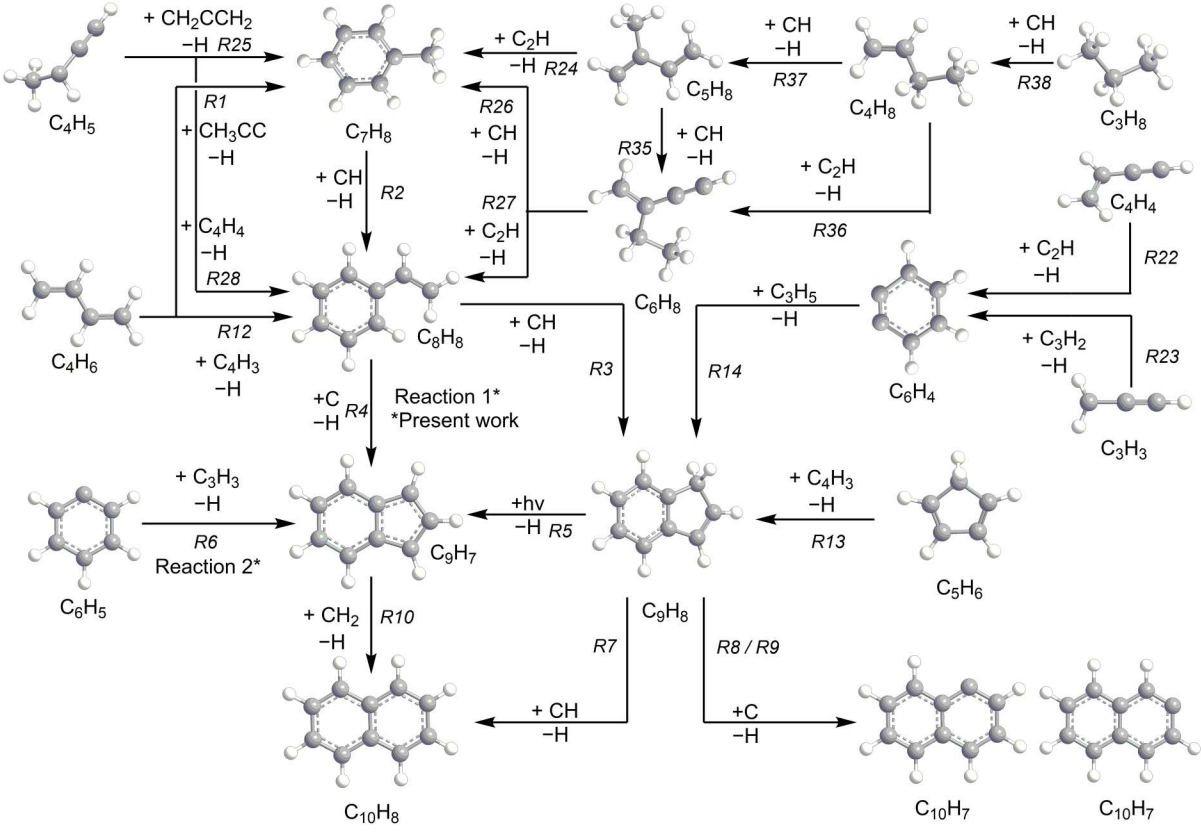

Fig. 5. Reaction network forming 1-indenyl. Compilation of key bimolecular reactions and photodissociation processes newly incorporated into the astrochemical model leading to the formation of 1-indenyl.

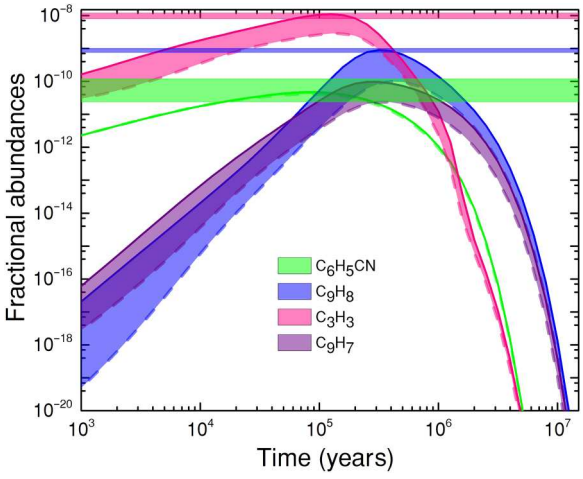

Fig. 6. Results of the astrochemical model for TMC-1. The fractional abundances of the gas-phase cyanobenzene (C_6H_5CN), indene (C_9H_8), propargyl (C_3H_3), and 1-indenyl (C_9H_7) are plotted as a function of time after the injection event. Astronomically observed fractional abundances, along with the uncertainties of cyanobenzene, indene, and propargyl, are visualized by the green-, blue-, and pink-colored horizontal bars.

exoergic reactions involving unconventional isomerization steps of the collision complexes via hydrogen shifts, ring closure/openings, and aromatization. These prerequisites represent fundamental criteria for both reactions to operate in cold molecular clouds such as TMC-1 and offer an unusual source of 1-indenyl ($C_9H_7^{\bullet}$) as precursors to a low-temperature route of PAHs in deep space, which may assist in deciphering the "lifetime paradox" of PAHs in the ISM. These findings also suggest that, upon reaction with atomic carbon and propargyl radicals, any vinyl side-chained six-membered aromatic ring or any aryl radical can be converted to a cyclopentadienyl moiety under low-temperature conditions (fig. S2), thus providing a facile and barrierless route of annulation of a benzene ring embedded in complex PAHs. These reaction routes are of particular importance as a critical sink of propargyl radicals detected with fractional abundances of $(1.0 \pm 0.2) \times 10^{-8}$ in TMC-1, which are unreactive with closed shell hydrocarbons under cold molecular cloud conditions revealing barriers to addition between 31 and 60 kJ mol^{-1} for, e.g., alkynes, alkenes, and aromatics (*62*–*64*). In low-temperature atmospheres of planets and their moons such as Titan and Triton, the outcome of these reactions is influenced by the atmospheric pressures. Whereas higher altitudes with pressures less than 10^{-3} torr support bimolecular reactions leading to 1-indenyl ($C_9H_7^{\bullet}$), third-body stabilization of the reaction intermediates in lower atmospheric layers leads to their stabilization and generation of distinct C_9H_8 isomers of 3-phenyl-1-propyne, phenylallene, and indene, which may act as fundamental molecular growth species in Titan's organic aerosol layers (*65*). Overall, our investigations provide a very first step to systematically elucidate the fundamental reaction pathways to RSFRs in low temperature environments as a critical prerequisite to their molecular mass growth processes to PAHs in extreme environments. Although the C_{2v} symmetric 1-indenyl ($C_9H_7^{\bullet}$) has not been detected yet in TMC-1, its resonance stabilization might lead to substantial fractional abundances, thus calling for future astronomical searches for 1-indenyl's astronomical identification. Combined with our extended astrochemical model, this identification would provide critical constraints on the largely elusive low-temperature molecular mass growth processes to aromatics in TMC-1 and act as a catalyst initiating advanced RSFR-triggered chain-propagating reactions eventually culminating in the rapid formation of carbonaceous nanostructures in deep space.

MATERIALS AND METHODS

Experimental methods: Carbon-styrene system

The gas phase reaction of ground-state atomic carbon (C; ^{3}P) with styrene ($C_6H_5C_2H_3$; X^1A') was carried out under single-collision conditions using a crossed molecular beam apparatus (*34*). The primary atomic carbon reactant was generated in situ via laser ablation of graphite exploiting the 266-nm output of an Nd:YAG laser at 8 to 10 mJ pulse^{-1} and seeding the ablated atoms in helium. A chopper wheel selected a part of the pulsed supersonic beam defined by the peak velocity v_p of 2534 ± 61 m s^{-1} and a speed ratio S of 2.2 ± 0.3. Under these experimental conditions, the carbon atoms produced are only in the ground electronic state (^{3}P) (*66*). The primary beam crossed a secondary beam of xenon-seeded (99.999%; Matheson) styrene (C_8H_8; >99%; TCI) defined by $v_p = 389 \pm 6$ m s^{-1} and $S = 28.0 \pm 0.4$ with a seeding fraction of 1% at a backing pressure of 550 torr. This resulted in a CM angle of 52.8 ± 0.6° and a collision energy of 35.4 ± 1.4 kJ mol^{-1}. The D3- and D5-styrene (98% D; CDN Isotopes) were used in the experiment to extract information on the position of the atomic hydrogen loss (table S1). After electron-impact ionization of the neutral products (80 eV, 2 mA), the ions were monitored using a quadrupole mass spectrometer operating in the TOF mode under ultrahigh-vacuum conditions (6×10^{-12} torr). After the normalization to CM angle and integration of the TOFs, the LAD distribution at well-defined m/z can be derived. A forward-convolution method based on Jacobian transformation is used to convert the data collected in the laboratory frame (LAD; TOFs) into the CM frame (*28*, *34*).

Experimental methods: Propargyl-phenyl system

The experiments were conducted at the Chemical Dynamics Beamline (9.0.2.) of the Advanced Light Source using a high-temperature chemical microreactor consisting of a resistively heated SiC tube of 20-mm heating length and 1-mm inner diameter. This device is located inside the source chamber of a molecular beam setup equipped with a Re-TOF-MS (*21*). The molecular beam apparatus is designed to study elementary chemical reactions ultimately leading to PAH growth in situ. In detail, phenyl ($C_6H_5^{\bullet}$) and propargyl ($C_3H_3^{\bullet}$) radials were prepared in situ via pyrolysis of nitrosobenzene (C_6H_5NO; ≥ 97%; Sigma-Aldrich) (*35*) and propargyl bromide (C_3H_3Br; > 98%; Sigma Aldrich) (*20*) precursors, respectively. The reactants were seeded in helium carrier gas at total pressures of 200 ± 10 torr at the reactor inlet. The propargyl bromide precursor was kept in a stainless-steel bubbler at a temperature of 199 K obtained in a dry ice–ethanol bath; the nitrosobenzene precursor was stored in a Swagelok particulate filter (Swagelok SS-6F-15) and cooled to 273 K via an ice bath. Both vessels were arranged in series: The helium carrier gas first passed through the liquid propargyl bromide sample; the resulting helium-seeded propargyl bromide gas mixture was then passed over the solid nitrosobenzene sample before entering the reactor. The temperature of the SiC tube was determined using a type C thermocouple to be 1373 ± 10 K. The

products formed in the reactor are entrained in a molecular beam, which passed a 2-mm skimmer located 10 mm downstream to the reactor; the beam then entered the main chamber, which houses the Re-TOF-MS. The neutral products within the supersonic molecular beam were photoionized in the extraction region of the mass spectrometer using quasi-continuous tunable synchrotron VUV light. VUV single-photon ionization represents essentially a fragment-free ionization technique and is a soft ionization method compared to the harsher conditions of electron impact ionization (*67*). The ions formed via soft photoionization were extracted and detected by a microchannel plate detector. Under our experimental condition, the residence time in the reactor tube is a few tens of microseconds (*68*, *69*). PIE curves, which report ion counts as a function of photon energy with a step interval of 0.05 eV at a well-defined *m*/*z*, were produced by integrating the signal recorded at the specific *m*/*z* for the species of interest. Control experiments were also proceeded by expanding neat helium carrier gas with each precursor separately into the resistively heated silicon carbide tube, but neither indene nor indenyl was detected. Last, reference PIE curves of helium-seeded 1-bromoindene (C_9H_7Br) (*46*) and 3-phenyl-1-propyne (C_9H_8; 97%; Sigma Aldrich) were recorded in the present work within the same experimental setup, respectively, whereas the PIE curve of phenylallene was provided by Kukkadapu *et al.* (*40*).

Computational methods: Electronic structure calculations

Electronic structure calculations in the present work were carried out on the triplet C_9H_8 potential energy surface accessed by the carbon-styrene reaction. In particular, geometries of the reactants, products, intermediates, and transition states involved in this reaction were optimized at the density functional theory B3LYP/6-311G(d,p) level (table S4) (*70*, *71*), with vibrational frequencies computed using the same theoretical approach. Single-point energies were further refined within the explicitly correlated CCSD(T)-F12/cc-pVTZ-F12 method (*43*, *72*), which normally provides the energetic parameters of local minima and transition states within "chemical accuracy" of ~5 kJ mol^{-1} for hydrocarbons in terms of average absolute deviations (*42*). The Gaussian 16 (*73*) and MOLPRO 2021 (*74*) program packages were used for the ab initio calculations. RRKM theory together with the steady-state approximation (*75*, *76*) implemented in our Unimol code (*77*) was applied to compute energy-dependent rate constants of all unimolecular reaction steps on the C_9H_8 triplet surface after the addition of the atomic carbon to styrene and to assess product branching ratios at zero-pressure limit under single-collision conditions.

Astrochemical modeling

To explore the chemistry leading to the 1-indenyl radical in the cold molecular cloud TMC-1, we constructed the chemical model by expanding the RATE12 network (*51*) with barrierless neutral-neutral reactions forming the 1-indenyl radical and their precursors. First, a time-dependent gas-phase model was operated until the chemistry evolves to the steady state, i.e., after typically 10^7 years. Simulations were also conducted in a separate model with the ice mantle species injected into the gas phase through reactive desorption until it reaches the steady state; this strategy was exploited successfully to demonstrate the key role of neutral-neutral reactions in the formation of benzene in TMC-1 (*52*). These results were then benchmarked with astronomical observations for cyanobenzene (C_6H_5CN), propargyl (C_3H_3), and indene (C_9H_8) to verify the predictive capabilities of the chemical network (Supplementary Materials).

Supplementary Materials

This PDF file includes:

Supplementary results
Figs. S1 to S7
Tables S1 to S4

REFERENCES AND NOTES

1. V. D. Knyazev, K. V. Popov, Kinetics of the self reaction of cyclopentadienyl radicals. *J. Phys. Chem. A* **119**, 7418–7429 (2015).
2. K. O. Johansson, M. P. Head-Gordon, P. E. Schrader, K. R. Wilson, H. A. Michelsen, Resonance-stabilized hydrocarbon-radical chain reactions may explain soot inception and growth. *Science* **361**, 997–1000 (2018).
3. L. Zhao, R. Kaiser, W. Lu, B. Xu, M. Ahmed, A. N. Morozov, A. M. Mebel, A. H. Howlader, S. F. Wnuk, Molecular mass growth through ring expansion in polycyclic aromatic hydrocarbons via radical–radical reactions. *Nat. Commun.* **10**, 1–7 (2019).
4. V. S. Krasnoukhov, M. V. Zagidullin, I. P. Zavershinskiy, A. M. Mebel, Formation of phenanthrene via recombination of indenyl and cyclopentadienyl radicals: A theoretical study. *J. Phys. Chem. A* **124**, 9933–9941 (2020).
5. S. Sinha, R. K. Rahman, A. Raj, On the role of resonantly stabilized radicals in polycyclic aromatic hydrocarbon (PAH) formation: Pyrene and fluoranthene formation from benzyl–indenyl addition. *Phys. Chem. Chem. Phys.* **19**, 19262–19278 (2017).
6. C. Wentrup, H.-W. Winter, D. Kvaskoff, C_9H_8 pyrolysis. *o*-Tolylacetylene, indene, 1-indenyl, and biindenyls and the mechanism of indene pyrolysis. *J. Phys. Chem. A* **119**, 6370–6376 (2015).
7. R. Zenobi, J.-M. Philippoz, R. N. Zare, P. R. Buseck, Spatially resolved organic analysis of the Allende meteorite. *Science* **246**, 1026–1029 (1989).
8. A. G. G. M. Tielens, Interstellar polycyclic aromatic hydrocarbon molecules. *Annu. Rev. Astron. Astrophys.* **46**, 289–337 (2008).
9. R. I. Kaiser, N. Hansen, An aromatic universe–A physical chemistry perspective. *J. Phys. Chem. A* **125**, 3826–3840 (2021).
10. E. R. Micelotta, A. P. Jones, A. G. G. M. Tielens, Polycyclic aromatic hydrocarbon processing in a hot gas. *Astron. Astrophys.* **510**, A36 (2010).
11. A. G. G. M. Tielens, The molecular universe. *Rev. Mod. Phys.* **85**, 1021–1081 (2013).
12. M. Frenklach, E. D. Feigelson, Formation of polycyclic aromatic hydrocarbons in circumstellar envelopes. *Astrophys. J.* **341**, 372–384 (1989).
13. D. A. García-Hernández, A. Manchado, P. García-Lario, L. Stanghellini, E. Villaver, R. A. Shaw, R. Szczerba, J. V. Perea-Calderón, Formation of fullerenes in H-containing planetary nebulae. *Astrophys. J. Lett.* **724**, L39–L43 (2010).
14. M. Tsuge, M. Bahou, Y.-J. Wu, L. Allamandola, Y.-P. Lee, The infrared spectrum of protonated ovalene in solid para-hydrogen and its possible contribution to interstellar unidentified infrared emission. *Astrophys. J.* **825**, 96 (2016).
15. N. Cox, J. Cami, L. Kaper, P. Ehrenfreund, B. Foing, B. Ochsendorf, S. Van Hooff, F. Salama, VLT/X-Shooter survey of near-infrared diffuse interstellar bands. *Astron. Astrophys.* **569**, A117 (2014).
16. A. G. G. M. Tielens, L. J. Allamandola, in *Cool Interstellar Physics and Chemistry* (Jenny Stanford Publishing, ed. 1, 2011), p 40.
17. M. Agúndez, C. Cabezas, B. Tercero, N. Marcelino, J. D. Gallego, P. de Vicente, J. Cernicharo, Discovery of the propargyl radical (CH_2CCH) in TMC-1: One of the most abundant radicals ever found and a key species for cyclization to benzene in cold dark clouds. *Astron. Astrophys.* **647**, L10 (2021).
18. M. Agúndez, N. Marcelino, C. Cabezas, R. Fuentetaja, B. Tercero, P. de Vicente, J. Cernicharo, Detection of the propargyl radical at λ 3 mm. *Astron. Astrophys.* **657**, A96 (2022).
19. A. M. Mebel, R. I. Kaiser, Formation of resonantly stabilised free radicals via the reactions of atomic carbon, dicarbon, and tricarbon with unsaturated hydrocarbons: Theory and crossed molecular beams experiments. *Int. Rev. Phys. Chem.* **34**, 461–514 (2015).
20. L. Zhao, W. Lu, M. Ahmed, M. V. Zagidullin, V. N. Azyazov, A. N. Morozov, A. M. Mebel, R. I. Kaiser, Gas-phase synthesis of benzene via the propargyl radical self-reaction. *Sci. Adv.* **7**, eabf0360 (2021).
21. R. I. Kaiser, L. Zhao, W. Lu, M. Ahmed, V. S. Krasnoukhov, V. N. Azyazov, A. M. Mebel, Unconventional excited-state dynamics in the concerted benzyl (C_7H_7) radical self-reaction to anthracene ($C_{14}H_{10}$). *Nat. Commun.* **13**, 1–8 (2022).

22. R. I. Kaiser, Y. T. Lee, A. G. Suits, Crossed-beam reaction of carbon atoms with hydrocarbon molecules. I. Chemical dynamics of the propargyl radical formation, $C_3H_3(X^2B_2)$, from reaction of $C(^3P_j)$ with ethylene, $C_2H_4(X^1A_g)$. *J. Chem. Phys.* **105**, 8705–8720 (1996).
23. W. D. Geppert, C. Naulin, M. Costes, G. Capozza, L. Cartechini, P. Casavecchia, G. Gualberto Volpi, Combined crossed-beam studies of $C(^3P_J) + C_2H_4 \rightarrow C_3H_3 + H$ reaction dynamics between 0.49 and 30.8 kJ mol^{-1}. *J. Chem. Phys.* **119**, 10607–10617 (2003).
24. J. A. Miller, M. J. Pilling, J. Troe, Unravelling combustion mechanisms through a quantitative understanding of elementary reactions. *Proc. Combust. Inst.* **30**, 43–88 (2005).
25. C. Yu, Z. Xiao, B. Dong, W. Chu, J. Guan, Z. Wang, Q. Zhang, Y. Chen, D. Zhao, Gas-phase optical spectra of the indenyl radical and its quantitative detection in a jet-stirred reactor. *J. Phys. Chem. A* **126**, 4630–4635 (2022).
26. G. da Silva, J. W. Bozzelli, Indene formation from alkylated aromatics: Kinetics and products of the fulvenallene + acetylene reaction. *J. Phys. Chem. A* **113**, 8971–8978 (2009).
27. S. Doddipatla, G. R. Galimova, H. Wei, A. M. Thomas, C. He, Z. Yang, A. N. Morozov, C. N. Shingledecker, A. M. Mebel, R. I. Kaiser, Low-temperature gas-phase formation of indene in the interstellar medium. *Sci. Adv.* **7**, eabd4044 (2021).
28. R. I. Kaiser, Experimental investigation on the formation of carbon-bearing molecules in the interstellar medium via neutral−neutral reactions. *Chem. Rev.* **102**, 1309–1358 (2002).
29. A. Coustenis, R. K. Achterberg, B. J. Conrath, D. E. Jennings, A. Marten, D. Gautier, C. A. Nixon, F. M. Flasar, N. A. Teanby, B. Bézard, The composition of Titan's stratosphere from Cassini/CIRS mid-infrared spectra. *Icarus* **189**, 35–62 (2007).
30. S. B. Morales, S. D. Le Picard, A. Canosa, I. R. Sims, Experimental measurements of low temperature rate coefficients for neutral–Neutral reactions of interest for atmospheric chemistry of Titan, Pluto and Triton: Reactions of the CN radical. *Faraday Discuss.* **147**, 155–171 (2010).
31. T. R. Melton, F. Inal, S. M. Senkan, The effects of equivalence ratio on the formation of polycyclic aromatic hydrocarbons and soot in premixed ethane flames. *Combust. Flame* **121**, 671–678 (2000).
32. N. M. Marinov, W. J. Pitz, C. K. Westbrook, A. M. Vincitore, M. J. Castaldi, S. M. Senkan, C. F. Melius, Aromatic and polycyclic aromatic hydrocarbon formation in a laminar premixed n-butane flame. *Combust. Flame* **114**, 192–213 (1998).
33. Y. Li, L. Zhang, T. Yuan, K. Zhang, J. Yang, B. Yang, F. Qi, C. K. Law, Investigation on fuel-rich premixed flames of monocyclic aromatic hydrocarbons: Part I. Intermediate identification and mass spectrometric analysis. *Combust. Flame* **157**, 143–154 (2010).
34. Z. Yang, G. R. Galimova, C. He, S. Doddipatla, A. M. Mebel, R. I. Kaiser, Gas-phase formation of 1, 3, 5, 7-cyclooctatetraene (C_8H_8) through ring expansion via the aromatic 1, 3, 5-cyclooctatrien-7-yl radical ($C_8H_9^{\bullet}$) transient. *J. Am. Chem. Soc.* **144**, 22470–22478 (2022).
35. L. Zhao, R. I. Kaiser, B. Xu, U. Ablikim, M. Ahmed, M. V. Zagidullin, V. N. Azyazov, A. H. Howlader, S. F. Wnuk, A. M. Mebel, VUV photoionization study of the formation of the simplest polycyclic aromatic hydrocarbon: Naphthalene ($C_{10}H_8$). *J. Phys. Chem. Lett.* **9**, 2620–2626 (2018).
36. D. S. N. Parker, R. I. Kaiser, On the formation of nitrogen-substituted polycyclic aromatic hydrocarbons (NPAHs) in circumstellar and interstellar environments. *Chem. Soc. Rev.* **46**, 452–463 (2017).
37. P. Hemberger, M. Steinbauer, M. Schneider, I. Fischer, M. Johnson, A. Bodi, T. Gerber, Photoionization of three isomers of the C9H7 radical. *J. Phys. Chem. A* **114**, 4698–4703 (2010).
38. Y. Li, J. Yang, Z. Cheng, Photonionization Cross Section Database (Version 2.0). NSRL, Hefei, China (2017); http://flame.nsrl.ustc.edu.cn/database/data.php.
39. M. J. S. Dewar, E. Haselbach, S. Worley, Calculated and observed ionization potentials of unsaturated polycyclic hydrocarbons; calculated heats of formation by several semiempirical scfmo methods. *Proc. R. Soc. London Ser. A* **315**, 431–442 (1970).
40. G. Kukkadapu, S. W. Wagnon, W. J. Pitz, N. Hansen, Identification of the molecular-weight growth reaction network in counterflow flames of the C_3H_4 isomers allene and propyne. *Proc. Combust. Inst.* **38**, 1477–1485 (2021).
41. T. M. Selby, F. Goulay, S. Soorkia, A. Ray, A. W. Jasper, S. J. Klippenstein, A. N. Morozov, A. M. Mebel, J. D. Savee, C. A. Taatjes, Radical–radical reactions in molecular weight growth: The phenyl + propargyl reaction. *J. Phys. Chem. A* **127**, 2577–2590 (2023).
42. J. Zhang, E. F. Valeev, Prediction of reaction barriers and thermochemical properties with explicitly correlated coupled-cluster methods: A basis set assessment. *J. Chem. Theory Comput.* **8**, 3175–3186 (2012).
43. T. B. Adler, G. Knizia, H.-J. Werner, A simple and efficient CCSD (T)-F12 approximation. *J. Chem. Phys.* **127**, 221106 (2007).
44. T. N. Le, H.-Y. Lee, A. M. Mebel, R. I. Kaiser, Ab initio MO study of the triplet C_3H_4 potential energy surface and the reaction of $C(^3P_j)$ with ethylene, C_2H_4. *J. Phys. Chem. A* **105**, 1847–H.-Y.1856 (2001).
45. D. C. Clary, N. Haider, D. Husain, M. Kabir, Interstellar carbon chemistry: Reaction rates of neutral atomic carbon with organic molecules. *Astrophys. J.* **422**, 416–422 (1994).
46. L. Zhao, M. B. Prendergast, R. I. Kaiser, B. Xu, W. Lu, U. Ablikim, M. Ahmed, A. D. Oleinikov, V. N. Azyazov, A. M. Mebel, Reactivity of the indenyl radical (C_9H_7) with acetylene (C_2H_2) and vinylacetylene (C_4H_4). *ChemPhysChem* **20**, 1437–1447 (2019).
47. P. Lindstedt, L. Maurice, M. Meyer, Thermodynamic and kinetic issues in the formation and oxidation of aromatic species. *Faraday Discuss.* **119**, 409–432 (2002).
48. A. N. Morozov, A. M. Mebel, Theoretical study of the reaction mechanism and kinetics of the phenyl+propargyl association. *Phys. Chem. Chem. Phys.* **22**, 6868–6880 (2020).
49. I. Hahndorf, Y. Lee, R. Kaiser, L. Vereecken, J. Peeters, H. Bettinger, P. Schreiner, P. V. R. Schleyer, W. Allen, H. Schaefer III, A combined crossed-beam, *ab initio*, and Rice–Ramsperger–Kassel–Marcus investigation of the reaction of carbon atoms $C(^3P_j)$ with benzene, C_6H_6 (X^1A_{1g}) and d6-benzene, C_6D_6 (X^1A_{1g}). *J. Chem. Phys.* **116**, 3248–3262 (2002).
50. D. E. Couch, G. Kukkadapu, A. J. Zhang, A. W. Jasper, C. A. Taatjes, N. Hansen, The role of radical-radical chain-propagating pathways in the phenyl+propargyl reaction. *Proc. Combust. Inst.* **39**, 643–651 (2023).
51. D. McElroy, C. Walsh, A. J. Markwick, M. A. Cordiner, K. Smith, T. J. Millar, The UMIST database for astrochemistry 2012. *Astron. Astrophys.* **550**, A36 (2013).
52. B. M. Jones, F. Zhang, R. I. Kaiser, A. Jamal, A. M. Mebel, M. A. Cordiner, S. B. Charnley, Formation of benzene in the interstellar medium. *Proc. Natl. Acad. Sci. U.S.A.* **108**, 452–457 (2011).
53. R. I. Kaiser, L. Zhao, W. Lu, M. Ahmed, M. M. Evseev, V. N. Azyazov, A. M. Mebel, R. K. Mohamed, F. R. Fischer, X. Li, Gas-phase synthesis of racemic helicenes and their potential role in the enantiomeric enrichment of sugars and amino acids in meteorites. *Phys. Chem. Chem. Phys.* **24**, 25077–25087 (2022).
54. A. J. Markwick, T. J. Millar, S. B. Charnley, On the abundance gradients of organic molecules along the TMC-1 ridge. *Astrophys. J.* **535**, 256–265 (2000).
55. B. A. McGuire, A. M. Burkhardt, S. Kalenskii, C. N. Shingledecker, A. J. Remijan, E. Herbst, M. C. McCarthy, Detection of the aromatic molecule benzonitrile (c-C_6H_5CN) in the interstellar medium. *Science* **359**, 202–205 (2018).
56. J. Cernicharo, M. Agúndez, R. I. Kaiser, C. Cabezas, B. Tercero, N. Marcelino, J. R. Pardo, P. de Vicente, Discovery of two isomers of ethynyl cyclopentadiene in TMC-1: Abundances of CCH and CN derivatives of hydrocarbon cycles. *Astron. Astrophys.* **655**, L1 (2021).
57. M. L. Sita, P. B. Changala, C. Xue, A. M. Burkhardt, C. N. Shingledecker, K. L. K. Lee, R. A. Loomis, E. Momjian, M. A. Siebert, D. Gupta, Discovery of interstellar 2-cyanoindene (2-C_9H_7CN) in GOTHAM observations of TMC-1. *Astrophys. J. Lett.* **938**, L12 (2022).
58. A. M. Burkhardt, K. L. K. Lee, P. B. Changala, C. N. Shingledecker, I. R. Cooke, R. A. Loomis, H. Wei, S. B. Charnley, E. Herbst, M. C. McCarthy, Discovery of the pure polycyclic aromatic hydrocarbon indene (c-C_9H_8) with GOTHAM observations of TMC-1. *Astrophys. J. Lett.* **913**, L18 (2021).
59. N. Balucani, O. Asvany, A. H. H. Chang, S. H. Lin, Y. T. Lee, R. I. Kaiser, H. F. Bettinger, P. V. R. Schleyer, H. F. Schaefer III, Crossed beam reaction of cyano radicals with hydrocarbon molecules. I. Chemical dynamics of cyanobenzene (C_6H_5CN; X^1A_1) and perdeutero cyanobenzene (C_6D_5CN; X^1A_1) formation from reaction of $CN(X^2\Sigma^+)$ with benzene C_6H_6 (X^1A_{1g}), and d6-benzene $C_6D_6(X^1A_{1g})$. *J. Chem. Phys.* **111**, 7457–7471 (1999).
60. M. N. McCabe, P. Hemberger, E. Reusch, A. Bodi, J. Bouwman, Off the beaten path: Almost clean formation of indene from the ortho-benzyne + allyl reaction. *J. Phys. Chem. Lett.* **11**, 2859–2863 (2020).
61. J. Kauffmann, G. Rajagopalan, K. Akiyama, V. Fish, C. Lonsdale, L. D. Matthews, T. Pillai, The Haystack telescope as an astronomical instrument. *Galaxies* **11**, 9 (2023).
62. A. Raj, M. J. Al Rashidi, S. H. Chung, S. M. Sarathy, PAH growth initiated by propargyl addition: Mechanism development and computational kinetics. *J. Phys. Chem. A* **118**, 2865–2885 (2014).
63. G. Da Silva, Mystery of 1-vinylpropargyl formation from acetylene addition to the propargyl radical: An open-and-shut case. *J. Phys. Chem. A* **121**, 2086–2095 (2017).
64. H. Jin, L. Xing, D. Liu, J. Hao, J. Yang, A. Farooq, First aromatic ring formation by the radical-chain reaction of vinylacetylene and propargyl. *Combust. Flame* **225**, 524–534 (2021).
65. S. Vinatier, B. Bézard, C. A. Nixon, A. Mamoutkine, R. C. Carlson, D. E. Jennings, E. A. Guandique, N. A. Teanby, G. L. Bjoraker, F. M. Flasar, Analysis of Cassini/CIRS limb spectra of Titan acquired during the nominal mission. *Icarus* **205**, 559–570 (2010).
66. Z. Yang, B.-J. Sun, C. He, J.-Q. Li, A. H. Chang, R. I. Kaiser, Gas-phase preparation of 1-germavinylidene (H_2CGe; X^1A_1), the isovalent counterpart of vinylidene (H_2CC; X^1A_1), via non-adiabatic dynamics through the elementary reaction of ground state atomic carbon (C; ^3P) with germane (GeH_4; X^1A_1). *J. Phys. Chem. Lett.* **14**, 430–436 (2023).
67. F. Qi, Combustion chemistry probed by synchrotron VUV photoionization mass spectrometry. *Proc. Combust. Inst.* **34**, 33–63 (2013).
68. Q. Guan, K. N. Urness, T. K. Ormond, D. E. David, G. Barney Ellison, J. W. Daily, The properties of a micro-reactor for the study of the unimolecular decomposition of large molecules. *Int. Rev. Phys. Chem.* **33**, 447–487 (2014).

69. M. V. Zagidullin, R. I. Kaiser, D. P. Porfiriev, I. P. Zavershinskiy, M. Ahmed, V. N. Azyazov, A. M. Mebel, Functional relationships between kinetic, flow, and geometrical parameters in a high-temperature chemical microreactor. *J. Phys. Chem. A* **122**, 8819–8827 (2018).
70. A. D. Becke, Density-functional thermochemistry. III. The role of exact exchange. *J. Chem. Phys.* **98**, 5648–5652 (1993).
71. C. Lee, W. Yang, R. G. Parr, Development of the Colle-Salvetti correlation-energy formula into a functional of the electron density. *Phys. Rev. B* **37**, 785–789 (1988).
72. G. Knizia, T. B. Adler, H.-J. Werner, Simplified CCSD (T)-F12 methods: Theory and benchmarks. *J. Chem. Phys.* **130**, 054104 (2009).
73. M. J. Frisch, G. W. Trucks, H. B. Schlegel, G. E. Scuseria, M. A. Robb, J. R. Cheeseman, G. Scalmani, V. Barone, B. Mennucci, G. A. Petersson, H. Nakatsuji, Gaussian 16, Revision C. 1; Gaussian Inc., Wallingford, CT, 2019.
74. H. J. Werner, P. J. Knowles, R. Lindh, F. R. Manby, M. Schütz, P. Celani, T. Korona, G. Rauhut, R. Amos, A. Bernhardsson, G. Knizia, A. Mitrushenkov, MOLPRO, version 2021.2, A Package of Ab Initio Programs; University of Cardiff, Cardiff, UK, 2021.
75. P. J. Robinson, K. A. Holbrook, *Unimolecular Reactions* (Wiley-Interscience, 1972).
76. V. V. Kislov, T. L. Nguyen, A. M. Mebel, S. H. Lin, S. C. Smith, Photodissociation of benzene under collision-free conditions: An ab initio/Rice–Ramsperger–Kassel–Marcus study. *J. Chem. Phys.* **120**, 7008–7017 (2004).
77. C. He, L. Zhao, A. M. Thomas, A. N. Morozov, A. M. Mebel, R. I. Kaiser, Elucidating the chemical dynamics of the elementary reactions of the 1-propynyl radical (CH_3CC; X^2A_1) with methylacetylene (H_3CCCH; X^1A_1) and allene (H_2CCCH_2; X^1A_1). *J. Phys. Chem. A* **123**, 5446–5462 (2019).

Acknowledgments: We thank P. Hemberger (LSF) for fruitful discussions on the PIE curves of 1-phenylpropargyl and 3-phenylpropargyl radicals. **Funding:** This work was supported by the U.S. Department of Energy, Basic Energy Sciences, by grant no. DE-FG02-03ER15411 to the University of Hawaii at Manoa and by grant no. DE-FG02-04ER15570 to the Florida International University. W.L. and M.A. were supported by the Director, Office of Science, Office of Basic Energy Sciences, of the U.S. Department of Energy under contract no. DE-AC02-05CH11231, through the Gas Phase Chemical Physics program of the Chemical Sciences Division. The Advanced Light Source (ALS) at Berkeley is also supported under contract no. DE-AC02-05CH11231. X.L. was supported by the Xinjiang Tianchi project (2019). **Author contributions:** R.I.K. designed the experiments; Z.Y., C.H., S.J.G., D.P., and W.L. performed experiments; Z.Y. and C.H. analyzed the data; M.A. supervised the experiments at the ALS; G.R.G. and A.M.M. carried out the theoretical analysis; X.L. conduct the modeling; all authors discussed the data; Z.Y. and R.I.K. wrote the paper. **Competing interests:** The authors declare that they have no competing interests. **Data and materials availability:** All data needed to evaluate the conclusions in the paper are present in the paper and/or the Supplementary Materials.

Submitted 2 May 2023
Accepted 7 August 2023
Published 8 September 2023
10.1126/sciadv.adi5060